

Improving Electrochemical Performance of $\text{Li}_{1.2}\text{Ni}_{0.13}\text{Co}_{0.13}\text{Mn}_{0.54}\text{O}_2$ Cathode Material by Al^{3+} Doping

Xinghua Liang^{1,*}, Hanjie Wu¹, Haiyan Chen²

¹ Guangxi Key Laboratory of Automobile Components and Vehicle Technology, Guangxi University of Science and Technology, Liuzhou 545600, China

² School of Materials and Energy, Guangdong University of Technology, Guangzhou 510006, China

*E-mail: liangxinghua888@163.com

Received: 26 July 2016 / Accepted: 5 September 2016 / Published: 10 October 2016

$\text{Li}_{1.2}\text{Ni}_{0.13}\text{Co}_{0.13}\text{Mn}_{0.54}\text{O}_2$ cathode materials doped with different Al^{3+} contents have prepared by high temperature solid state method, which are studied using X-ray diffractometry, X-ray photoelectron spectroscopy, Infrared absorption spectrum, scanning electron microscopy, electron diffraction spectroscopy (EDS), high resolution transmission electron micrograph (HRTEM), charge-discharge measurements and electrochemical impedance spectroscopy. Al doped $\text{Li}_{1.2}\text{Ni}_{0.13}\text{Co}_{0.13}\text{Mn}_{0.54}\text{O}_2$ with hexagonal crystal system structure and layered structure of $\alpha\text{-NaFeO}_2$ indicates better crystal stability and more excellent energy storage systems. The Al^{3+} doped cathode materials can indicate bigger discharged capacities, better cycling stability and rate performance compared with the pristine cathode material according to the results of kinds of characterization technique support each other, it can prove successful a lot of Al^{3+} doping into $\text{Li}_{1.2}\text{Ni}_{0.13}\text{Co}_{0.13}\text{Mn}_{0.54}\text{O}_2$ lattice rather than generating new phase structure. This superior electrochemical performance of $\text{Li}_{1.2}\text{Ni}_{0.13}\text{Co}_{0.13}\text{Mn}_{0.54}\text{O}_2$ cathode material is attributed to the Al^{3+} doping.

Keywords: Electrochemical performance; $\text{Li}_{1.2}\text{Ni}_{0.13}\text{Co}_{0.13}\text{Mn}_{0.54}\text{O}_2$; Al^{3+} doping

1. INTRODUCTION

Lithium ion batteries is a new generation of secondary battery after the lead-acid batteries, nickel cadmium batteries and nickel-metal hydride batteries. With the rapid development of portable electronic devices [1], all-electric vehicles (EVs) and plug-in hybrid electric vehicles (PHEVs) [2], the demands for Li-ion batteries (LIBs) with high specific capacity, high working voltage, wide working temperature range, long cycle life, no memory effect, and harmless to the environment, etc [3-6]. LIBs are considered to be a green power of the 21st century and have promoted considerable efforts to develop alternative cathode materials [7-10]. $\text{Li}_{1.2}\text{Ni}_{0.13}\text{Co}_{0.13}\text{Mn}_{0.54}\text{O}_2$ [11] (LNCMO) is a promising cathode material owing to its high density, low pollution, and superior electrochemical performance. In

order to, the Li-rich cathode material of layered LiMO_2 and Li_2MnO_3 ($\text{M}=\text{Ni}, \text{Co}, \text{Mn}$) [12] have attracted a lot of attention in a recent period, and the Li-rich layered oxide $x\text{Li}_2\text{MnO}_3 \cdot (1-x)\text{LiMaO}_2$ ($\text{Ma}=\text{Co}, \text{Ni}, \text{Mn}$) [13] has been regarded as one of the most potential cathode materials of newest generation lithium ion batteries, due to they could show much bigger discharge capacity ($>200 \text{ mAh} \cdot \text{g}^{-1}$) with outstanding decreased resource compared to the LiCoO_2 [14] materials. In recently for a period of time, some researches payed attention to the Li-rich manganese layered oxides which showed a discharge capacity scope of $200\text{-}300 \text{ mAh} \cdot \text{g}^{-1}$ [15-20]. The oxygen ion conductivity and oxygen vacancies can be improved significantly with Al_2O_3 doping elements, and ionic conductivity can enhance electrochemical performance [21-25].

In this work, $\text{Li}_{1.2}\text{Ni}_{0.13}\text{Co}_{0.13}\text{Al}_x\text{Mn}_{0.54-x}\text{O}_2$ (LNCAMO) cathode material has prepared by high temperature solid state method, which is widely used in the lithium ion battery industry [26-32].

2. EXPERIMENTAL

2.1. Preparation of materials

The $\text{Li}_{1.2}\text{Ni}_{0.13}\text{Co}_{0.13}\text{Al}_x\text{Mn}_{0.54-x}\text{O}_2$ ($x=0, 0.01, 0.02, 0.03$) mixed materials were prepared by a high temperature solid state synthesized method. The industrial raw materials are $\text{LiOH} \cdot \text{H}_2\text{O}$ (56.5%, purity), $\text{Ni}(\text{CH}_3\text{COO})_2 \cdot 4\text{H}_2\text{O}$ (98%, purity), $\text{Al}_2\text{O}_3 \cdot 3\text{H}_2\text{O}$ (98%, purity), $\text{Mn}(\text{CH}_3\text{COO})_2 \cdot 4\text{H}_2\text{O}$ (99%, purity), $\text{Co}(\text{CH}_3\text{COO})_2 \cdot 4\text{H}_2\text{O}$ (99.5%, purity), were mixed in 250 ml distilled water with continuous whipping in 10 h, and then rubbing for 2 h. These samples were burned at 550°C for 6 h and sintered at 900°C for 12 h in oxygen to get pure LNCAM powders. The original and modified samples were marked as LNCAM0, LNCAM1, LNCAM2 and LNCAM3 ($x=0, 0.01, 0.02, 0.03$ of material $\text{Li}_{1.2}\text{Ni}_{0.13}\text{Co}_{0.13}\text{Al}_x\text{Mn}_{0.54-x}\text{O}_2$), respectively.

2.2. Material characterization

The structure of $\text{Li}_{1.2}\text{Ni}_{0.13}\text{Co}_{0.13}\text{Al}_x\text{Mn}_{0.54-x}\text{O}_2$ (XRD) using DX-2700 XRD ($\lambda=1.5406\text{\AA}$) scope of $10^\circ < 2\theta < 90^\circ$ and sweep frequency of $3^\circ/\text{min}$. XPS (PHI 5000 VersaProbe II) was carried out electron spectrosscopy for chemical analysis. The micrographs of samples were analyzed by scanning electron microscopy (EVO-18 SEM). The structure of cathode materials were analysed by high resolution transmission electron microscopy (JEM-2100F). Technology of FTIR (BIO-RED FTS300) can be used to detect a variety of chemical molecules, and for different kings of chemicals at the same time has a fairly high rate of identification.

2.3. Electrochemical characterization

Electrochemical properties were characterized based on CR2032 coin-type half-cell. Cathode materials $\text{Li}_{1.2}\text{Ni}_{0.13}\text{Co}_{0.13}\text{Al}_x\text{Mn}_{0.54-x}\text{O}_2$, graphitized carbon black, and PVDF adhesive are a blend rate of 7.5:1.5:1 in NMP spirit and mixed for well-distributed size. And then the size was expanded carry

out an aluminium foil and baked at 80°C for 10 h. Electrolyte is ethylene carbonate (EC) and dimethyl carbonate (DMC) (EC/DMC = 1.2:1 by bulk) of 1 mol·L⁻¹ LiPF₆.

The assemble cells are charged and discharged potential scope of 2.0-4.8 V with Neware Battery Test Station (CT3008W-5V5mA-S4, CHINA). Electrochemical impedance spectroscopy analysis were carried out an workstation (CHI660E, CHINA). EIS measurement was a rate scope of 100 kHz-0.001 Hz.

3. RESULTS AND DISCUSSION

3.1. Physical properties of LNCAM cathode materials

It has been shown XRD spectra of cathode material Li_{1.2}Ni_{0.13}Co_{0.13}Al_xMn_{0.54-x}O₂ in Fig. 1 . All the patterns can quoted according to a hexagonal crystal system of α-NaFeO₂ with space system (R $\bar{3}$ m). The division of (006)/(012) and (018)/(110) reflection angles of samples shows the formation of excellent layered crystal system. This weak super-lattice angles indicate at scope of 20-25°, consistent with basic on Li⁺ and Mn⁴⁺ of Li_{1.2}Ni_{0.13}Co_{0.13}Mn_{0.54}O₂ structure described by the space group (C2/m). Al³⁺ doping didn't affect the pristine phase structure. In addition, other impurities are not detected, especially Al related impurities didn't found in the Al³⁺ doping samples, preliminary it show that doping atoms may success with Li_{1.2}Ni_{0.13}Co_{0.13}Mn_{0.54}O₂. Besides, all the diffraction peaks of Fig. 1 are nearly uniform for these samples, it can be seen Al³⁺ doping has no significant impact in the bulk crystallo-graphic crystal of Li_{1.2}Ni_{0.13}Co_{0.13}Mn_{0.54}O₂ [33]. Table 1 shows lattice parameters of the Li_{1.2}Ni_{0.13}Co_{0.13}Al_xMn_{0.54-x}O₂ samples calculated according to the Fig. 1. XRD data. The lattice parameters, a, c, c/a was found that the unit cell volume of Al³⁺ doping samples is lower than pristine, this may be due to the radius of Al³⁺ (0.057 nm) is less than the Ni²⁺ (0.069 nm), and a large number of Mn²⁺ was replaced by the Al³⁺, leading to cell shrinkage. Repair not only indirectly proves that the Al³⁺ has been successfully doped to Li_{1.2}Ni_{0.13}Co_{0.13}Mn_{0.54}O in the lattice, but semi quantitatively reflects the relevant Al³⁺ doping on the microstructure effect of material crystal.

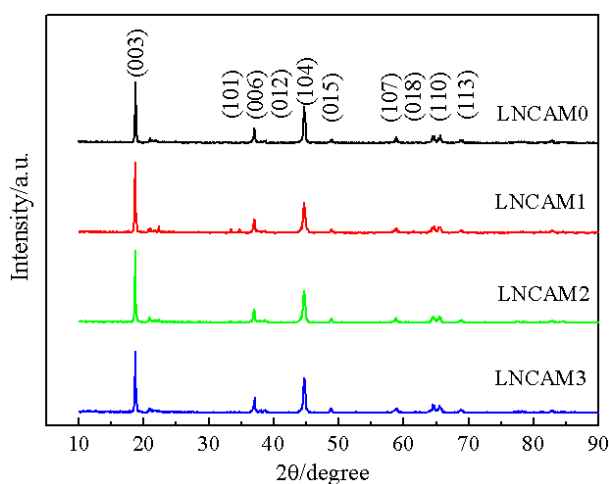
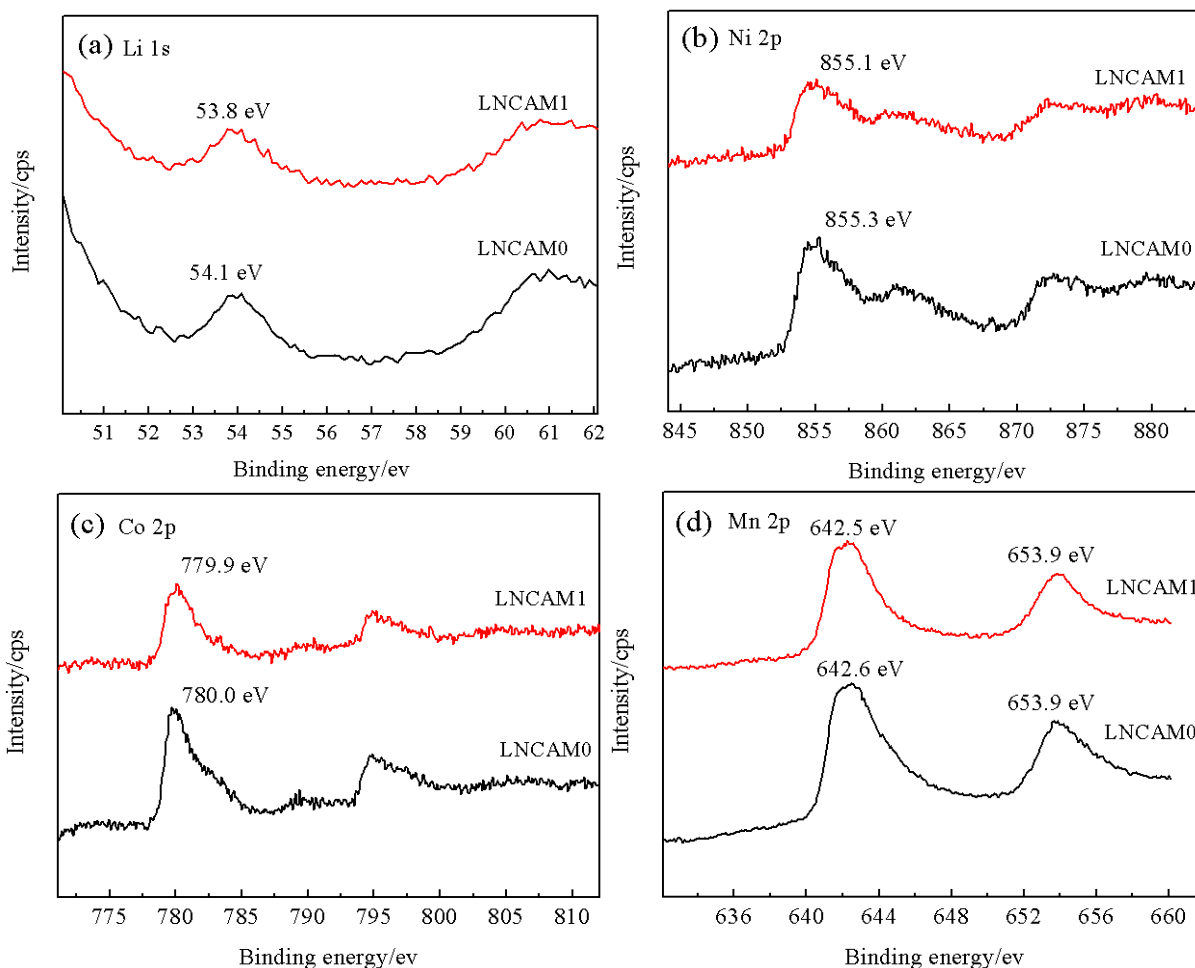


Figure 1. XRD patterns of Li_{1.2}Ni_{0.13}Co_{0.13}Al_xMn_{0.54-x}O₂ (x=0, 0.01, 0.02, 0.03).

Table 1. Lattice parameters of $\text{Li}_{1.2}\text{Ni}_{0.13}\text{Co}_{0.13}\text{Al}_x\text{Mn}_{0.54-x}\text{O}_2$ ($x=0, 0.01, 0.02, 0.03$)

Al(x)	a (Å)	c (Å)	c/a	$I_{(003)}/I_{(104)}$	Cell Volume (Å) ³
0	2.8631	14.3865	5.02467	2.01	101.18
0.01	2.8610	14.3604	5.02364	1.94	100.14
0.02	2.8581	14.3581	5.01921	1.83	99.75
0.03	2.8538	14.2807	5.00402	1.72	99.48

XPS was applied due to judge the oxidation states of different ions. The XPS spectra of Al^{3+} doping and pristine sample for the Li 1s, Mn 2p, Co 2p, Ni 2p, O 1s and Al 2p peaks are shown in Fig. 2(a) to (f), it has not chemical shift after Al^{3+} doping, indicating the chemical states of Li, Ni, Co, Mn, and O elements maintain stability and in agreement the XRD results. About the interim metal elements, no obvious variation of the XPS peaks location were surveyed in these samples [34]. Therefore, the intensities of various peaks of Li 1s, Ni 2p, Co 2p, and Mn 2p reduce due to Al^{3+} doping.



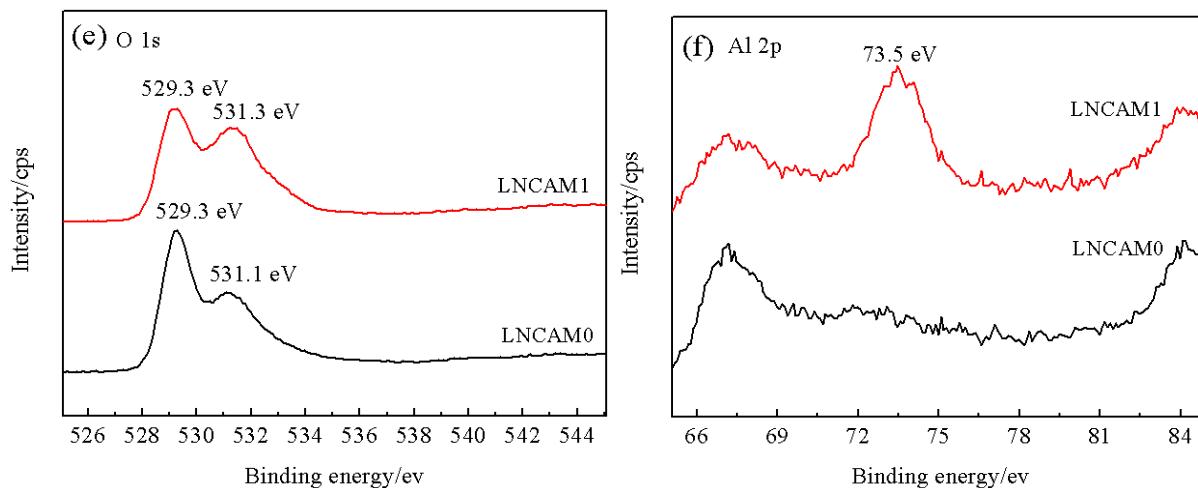


Figure 2. XPS spectra curves for ions (Li, Ni, Co, Mn, O, Al) in Al³⁺ doping and the pristine sample.

Fig. 2(f) shows the Al 2p peak correspond to 73.5 eV, it can also account for Al is 3⁺, as reported elsewhere. So that the data also indicates support an existence of the most number of Al³⁺ in the doped sample. This result is corresponding to a series of variation of lattice constants of XRD, It can be seen that the Al³⁺ have been successfully entered into the lattice structure of Li-rich cathode material.

Fig. 3 shows spectrum analysis of infrared absorption spectrum of Li_{1.2}Ni_{0.13}Co_{0.13}Al_xMn_{0.54-x}O₂ (x=0, 0.01, 0.02, 0.03), 609.26 and 510.32 cm⁻¹ of the band peaks correspond to dissymmetry stretching vibration in Mn (IV)-O and Mn (III)-O of Li-rich cathode material structure (Mn (IV) O₆ and Mn (III) O₆ octahedral), respectively, 890.74 and 1491.85 cm⁻¹ of the band peaks correspond to dissymmetry stretching vibration in Li-O and Al-O of Li_{1.2}Ni_{0.13}Co_{0.13}Al_xMn_{0.54-x}O₂ (x=0, 0.01, 0.02, 0.03) (LiO₄ and Al₂O₃ tetrahedron), which indicates that the Al³⁺ doping successfully entered Li_{1.2}Ni_{0.13}Co_{0.13}Mn_{0.54}O of lattice.

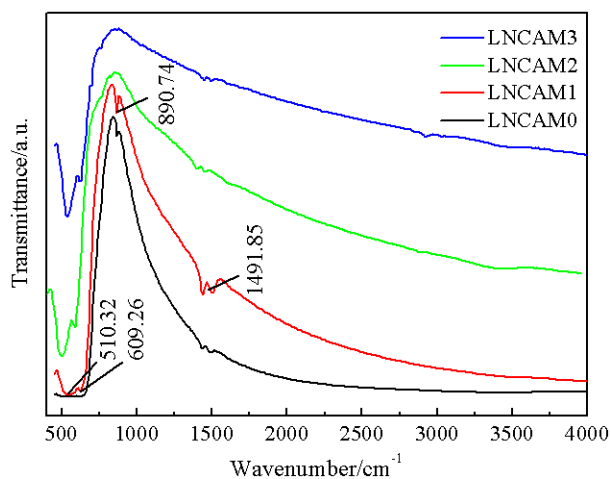


Figure 3. Infrared absorption spectrum of Li_{1.2}Ni_{0.13}Co_{0.13}Al_xMn_{0.54-x}O₂ (x=0, 0.01, 0.02, 0.03).

Fig. 4 (a)-(d) shows the SEM images of $\text{Li}_{1.2}\text{Ni}_{0.13}\text{Co}_{0.13}\text{Al}_x\text{Mn}_{0.54-x}\text{O}_2$ ($x=0, 0.01, 0.02, 0.03$) show scope of 200-400 nm of clear the size of the particles. Higher Al doping could have a greater impact $\text{Li}_{1.2}\text{Ni}_{0.13}\text{Co}_{0.13}\text{Mn}_{0.54}\text{O}_2$ main particle morphology. Besides, the distinct compare with the form among these samples and Al^{3+} doping samples change better at it surface [35]. Fig. 5 EDS for the samples in different regions, to judge the existence of and the percentage of O, Al, Mn, Ni, Co ions. Element proportion of every sample is listed in Table 2.

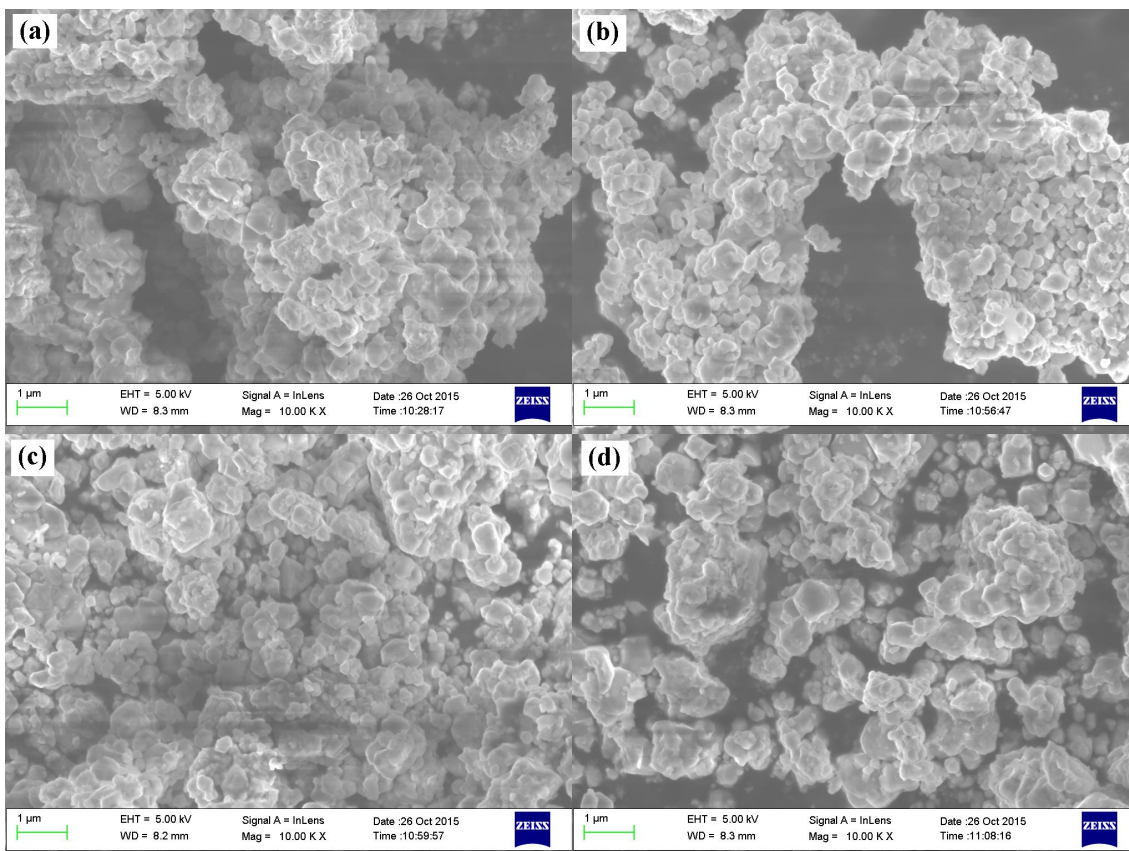


Figure 4. SEM of $\text{Li}_{1.2}\text{Ni}_{0.13}\text{Co}_{0.13}\text{Al}_x\text{Mn}_{0.54-x}\text{O}_2$ (a) $x=0$, (b) $x=0.01$, (c) $x=0.02$, (d) $x=0.03$.

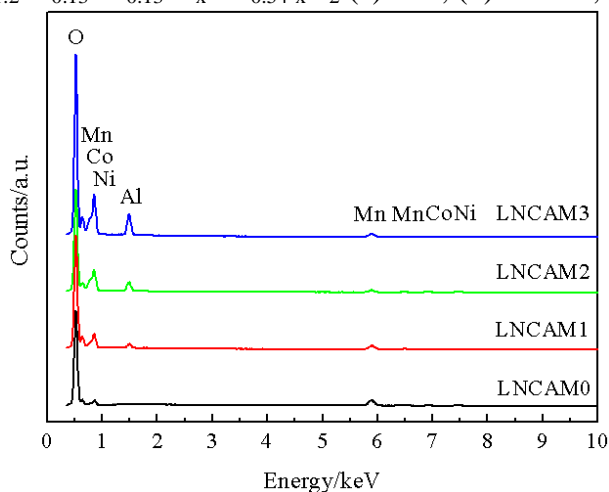


Figure 5. EDS of $\text{Li}_{1.2}\text{Ni}_{0.13}\text{Co}_{0.13}\text{Al}_x\text{Mn}_{0.54-x}\text{O}_2$ (a) $x=0$, (b) $x=0.01$, (c) $x=0.02$, (d) $x=0.03$.

Table 2. Proportion of atom O, Al, Mn, Co and Ni at $\text{Li}_{1.2}\text{Ni}_{0.13}\text{Co}_{0.13}\text{Al}_x\text{Mn}_{0.54-x}\text{O}_2$ ($x=0, 0.01, 0.02, 0.03$)

Element	LNCAM0 (%)	LNCAM1 (%)	LNCAM2 (%)	LNCAM3 (%)
O	72.84	70.17	69.11	67.35
Al	0	1.35	2.27	3.44
Mn	18.00	17.40	16.14	15.01
Co	3.46	4.73	4.76	5.72
Ni	5.70	6.35	7.72	8.48
Sum	100	100	100	100

Further combining with XRD analysis of Fig. 1, the results of kinds of characterization technique support each other, it can prove successful a lot of Al^{3+} doping into $\text{Li}_{1.2}\text{Ni}_{0.13}\text{Co}_{0.13}\text{Mn}_{0.54}\text{O}_2$ lattice rather than generating new phase structure.

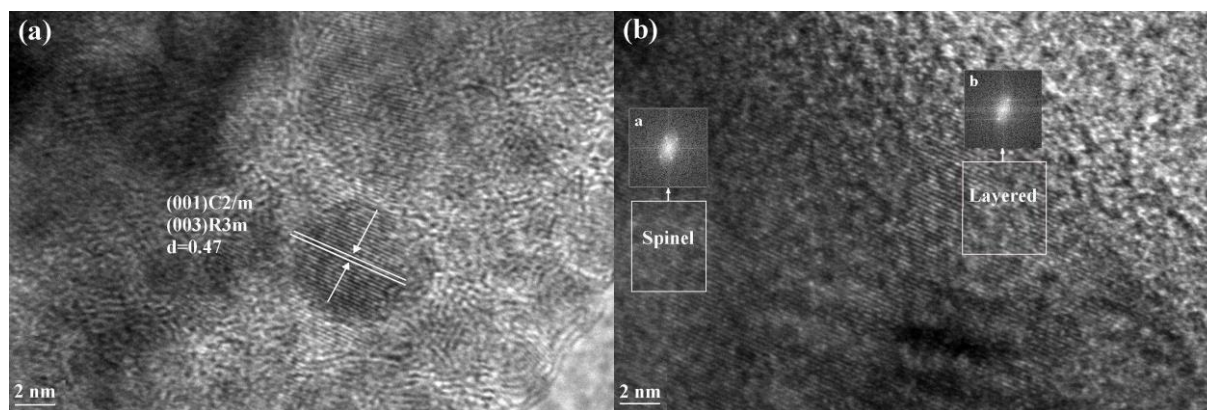
**Figure 6.** HR-TEM images(a) and SAED images(b) of Al^{3+} doping sample.

Fig. 6(a) shows HR-TEM images of as-synthesized material, from which distinct interplanar spacing with $d=0.47$ nm can be observed. On second thought would be needed to rate of return any results about delithium crystal with accumulation faults or hexagonal system crystal [36]. This value coincides with the interplanar distance of (001) plane of Li_2MnO_3 and/or the (003) plane of LiMO_2 . Crystal phase and SAED images(b) of Al^{3+} doping sample was indicated in Fig. 6(b), layered phase and spinel phase could observed in the Al^{3+} doping sample, which agrees with the XRD analysis results.

3.2 Electrochemical performance

As shown in Fig. 7, Specific capacity of Al^{3+} doping sample was slightly lighter than cycling performance of pristine sample, this is because a surfeit of Al_2O_3 of Al^{3+} doping sample appear in the surface of $\text{Li}_{1.2}\text{Ni}_{0.13}\text{Co}_{0.13}\text{Mn}_{0.54}\text{O}_2$ and hinder Li^+ migration, so that it result in a decline in specific capacity. Which account for pristine electrode delivers the biggest discharge capacity first cycle. This is attracted by the industrial raw materials, Li-rich cathodes produce Li_2O and form the SEI film, the

film of conductive materials capacity is a contribution.

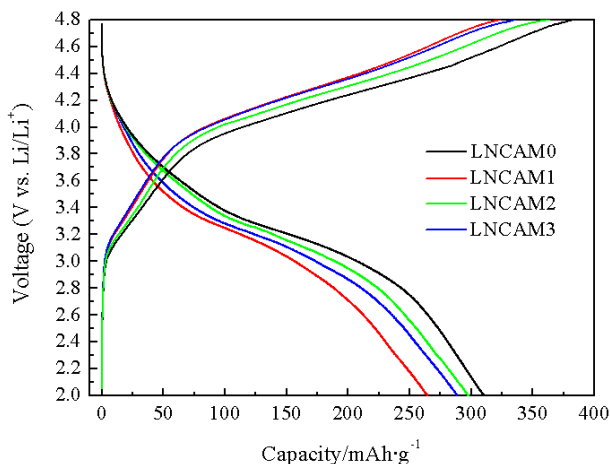


Figure 7. Charge and discharge capacity of different doping content at 0.1C of first cycle.

Fig. 8 is different ratio of discharge capacity at 0.1 C, 0.2 C, 0.3 C, 0.5 C, 1 C, 2 C and 3 C of the sample LNCAM0, LNCAM1, LNCAM2 and LNCAM3. Discharge specific capacity of Al^{3+} doping of Li-rich cathode material is higher than pristine sample with the increase of the charge and discharge ratio. Discharge specific capacity at sample LNCAM0 fell sharply is $100 \text{ mAh}\cdot\text{g}^{-1}$ in 3 C ratio; LNCAM1, LNCAM2 and LNCAM3 Sample are $203 \text{ mAh}\cdot\text{g}^{-1}$, $231 \text{ mAh}\cdot\text{g}^{-1}$ and $225 \text{ mAh}\cdot\text{g}^{-1}$ with 3 C ratio, which shows Al^{3+} doping can improve ratio performance with $Li_{1.2}Ni_{0.13}Co_{0.13}Mn_{0.54}O_2$. After grate rate charge and discharge test backing to 0.1 C ratio, material discharge specific capacity fell slightly, so grate ratio after the charge and discharge does not have great influence on the material structure. This behaviour is typical of spinel material, in the process of material circulation integrate fault [37].

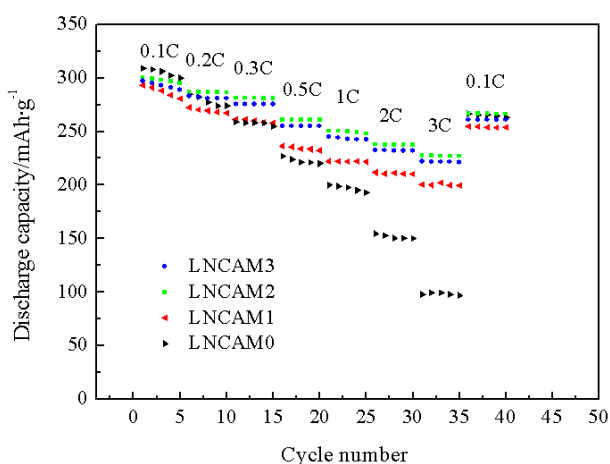


Figure 8. The rate performance of different samples at different rates.

The capacity decrease fast from Fig. 9. However, Al^{3+} doping samples indicate improvement

capacity, which maintain 96% in the following 100 cycles. Therefore, The discharge capacity, rate capacity and cycling capacity of $\text{Li}_{1.2}\text{Ni}_{0.13}\text{Co}_{0.13}\text{Al}_{0.02}\text{Mn}_{0.52}\text{O}_2$ are better than other samples. This is due to the following respects: 1) Al^{3+} doping can inhibit grain growth and reduce grain size, which would be helpful to the diffusion of Li^+ ; 2) lattice number of LNCAM0 is small, which can help stabilize the spinel crystal structure, thus to some extent inhibit electrode materials from the cubic lattice to square lattice Jahn-Teller effect, so that it can improve electrochemical performance of LNCAM0. 3) Al^{3+} doping can improve spinel LNCAM0 (001) plane with Mn^{2+} valence state, but the surface Mn^{3+} content is reduced, thereby reducing the occurrence of Mn^{3+} disproportionation reaction and amount of Mn^{3+} dissolved, so that it can improve the cycle performance of LNCAM0.

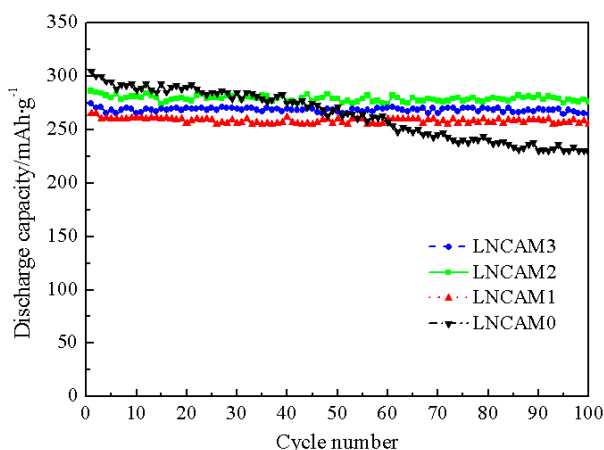


Figure 9. The cycling performance of different doping content at 0.1C and at first cycle.

Fig. 10 presents the EIS curve and fitting data in Table 3 of the $\text{Li}_{1.2}\text{Ni}_{0.13}\text{Co}_{0.13}\text{Al}_x\text{Mn}_{0.54-x}\text{O}_2$ electrode. The semicircle should correspond to the transfer resistance (R_{ct}). Li-rich cathodes produce Li_2O and form the SEI film, the film of conductive materials capacity is a contribution. Pristine has smaller particle size at the solution resistance (R_s) after 1st, but agglomerations that Al doped particles decrease quickly at (R_s) after 100th, and specially $\text{Li}_{1.2}\text{Ni}_{0.13}\text{Co}_{0.13}\text{Al}_{0.02}\text{Mn}_{0.52}\text{O}_2$ particle of porous hollow phase could show higher electrochemical performance. The Al^{3+} doping samples randomized controlled trial is less than the original sample, because of improved electronic conductivity, this suggests that the resulting efficient function and improve the dynamic enhancement [38]. Because of Mn dissolution of material, so $\alpha\text{-NaFeO}_2$ structure stability decrease and it cause impedance increase rapidly, after surface of cathode materials doping suitable amount of Al^{3+} , with the contact between cathode materials and electrolyte decreasing, reducing electrode/electrolyte decomposition, and impedance growth is slower; Especially Al^{3+} doping samples, besides reducing the dissolution of Mn doping layer, a small amount of the solid solution formation of Li - Ni - Co - Al - Mn - O make the structure more stable, so the impedance of the slowest growth rate. When excessive amounts of Al^{3+} doping, Al^{3+} covering on the surface of samples and hindering the Li^+ embedded and emergence, result in rising impedance.

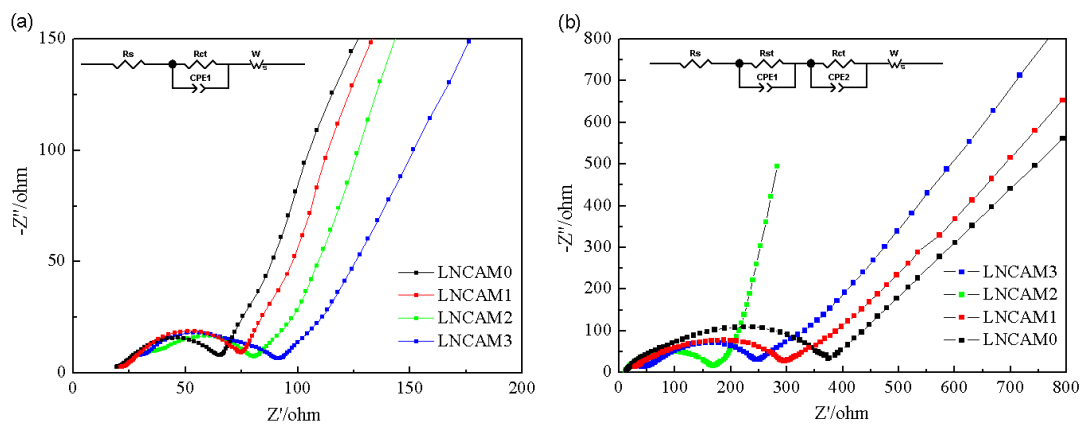


Figure 10. The EIS curve of electrodes after first cycle and 100th cycle for $\text{Li}_{1.2}\text{Ni}_{0.13}\text{Co}_{0.13}\text{Al}_x\text{Mn}_{0.54-x}\text{O}_2$.

Table 3. Lattice parameters of $\text{Li}_{1.2}\text{Ni}_{0.13}\text{Co}_{0.13}\text{Al}_x\text{Mn}_{0.54-x}\text{O}_2$ ($x=0, 0.01, 0.02, 0.03$)

Samples	Before cycling		After 100th cycles		
	Rs	Rct	Rs	Rst	Rct
LNCAM0	2.19	91.31	2.05	273.65	100.2
LNCAM1	3.42	80.22	1.92	204.94	91.47
LNCAM2	4.85	74.72	1.70	138.42	83.16
LNCAM3	5.61	65.26	1.87	172.98	74.95

4. CONCLUSION

In summary, $\text{Li}_{1.2}\text{Ni}_{0.13}\text{Co}_{0.13}\text{Al}_x\text{Mn}_{0.54-x}\text{O}_2$ ($x=0, 0.01, 0.02, 0.03$) cathode materials have been prepared by high temperature solid state method. It has confirmed the Al^{3+} doping into the structure of pristine. Through the analysis of experimental data shows discharged capacities, rate performance and cyclic stability in $\text{Li}_{1.2}\text{Ni}_{0.13}\text{Co}_{0.13}\text{Mn}_{0.54}\text{O}_2$ was improved with Al^{3+} doping and aluminum doping can significantly improve polarization increase and decrease Ac impedance during charge and discharge. Al^{3+} doping $\text{Li}_{1.2}\text{Ni}_{0.13}\text{Co}_{0.13}\text{Mn}_{0.54}\text{O}_2$ shows a better rate capacity, with the discharge specific capacity of $\text{Li}_{1.2}\text{Ni}_{0.13}\text{Co}_{0.13}\text{Al}_x\text{Mn}_{0.54-x}\text{O}_2$ ($x=2$) is $304 \text{ mAh}\cdot\text{g}^{-1}$, $278 \text{ mAh}\cdot\text{g}^{-1}$, $274 \text{ mAh}\cdot\text{g}^{-1}$, $253 \text{ mAh}\cdot\text{g}^{-1}$ and $250 \text{ mAh}\cdot\text{g}^{-1}$, $248 \text{ mAh}\cdot\text{g}^{-1}$, $241 \text{ mAh}\cdot\text{g}^{-1}$ at 0.1C, 0.2C, 0.3C, 0.5C, 1C, 2C and 3C.

ACKNOWLEDGEMENT

This project was supported by the Fund and Opening Project of Guangxi Key Laboratory of Automobile Components and Vehicle Technology, Guangxi University of Science and Technology (No.15-A-03-01, 2015KFZD02). It was supported by the Innovation Project of GuangXi University of Science and Technology Graduate Education(GKYC201617).

References

1. J. Liu, A. Manthiram, *J. Mater. Chem.*, 20 (2010) 3950-3964.

2. C. J. Jafta, K. I. Ozoemena, *Electrochimica Acta*, 80 (2012) 411-422.
3. Q. Li, G. Li, *ACS Appl. Mat. Interfaces*, 6 (2014) 10328-10334.
4. F. He, X. Wang, *Electrochimica Acta*, 153 (2015) 484-491.
5. L. Ban, Y. Yin, *Electrochimica Acta*, 180 (2015) 218-226.
6. X. Li, Z. Xie, *Electrochimica Acta*, 174 (2015) 1122-1130.
7. H. Chen, Q. Hu, *Ceramics International*, 42(2016) 263-269.
8. Y. Zang, C. X. Ding, *Electrochimica Acta*, 168(2015) 234-239.
9. L. Li, B. H. Song, *J. Power Sources*, 283(2015) 163-170.
10. D. T. Liu, W. X. Ding, *Applied Mechanics and Materials*, 543(2014) 1351-1354.
11. C. Lu, H. Wu, *J. Power Sources*, 267(2014) 682-691.
12. C. T. Hsieh, H. H. Hsu, *Solid State Ionics*, 270(2015) 39-46.
13. M. M. Thackeray, S. H. Kang, *Journal of Materials Chemistry*, 30 (2007) 3112-3125.
14. C. S. Johnson, N. Li, *Electrochemistry Communications*, 5 (2005) 528-536.
15. G. V. Zhuang, G. Y. Chen, *J. Power Sources*, 134 (2004) 291-296.
16. X. Wei, S. Zhang, *Electrochim. Acta*, 107 (2013) 547-553.
17. H. G. Wu, C. Prem, H. S. Chang, *J. Chin. Chem. Soc.*, 59 (2012) 1264-1269.
18. H. Koga, *Croguennec. L.*, 160 (2013) A786-A792.
19. X. Zhao, J. J. Wang, *Chin. Chem. Soc.*, 61 (2014) 1071-1083.
20. Y. S. Jung, A. S. Cavanagh, *J. Electrochem. Soc.*, 158 (2011) A1298-A1302.
21. Q. Y. Wang, J. J. Liu, *Mater. Chem.*, 19 (2009) 4963-4968.
22. Y. Hu, G. Wang, *Ceramics International*, 42(2016) 11422-11428.
23. X. Jin, Q. Xu, *Electrochimica Acta*, 136 (2014) 19-26.
24. T. Zhao, S. Chen, *Journal of Power Sources*, 228 (2013) 206-213.
25. J. M. Zheng, X. B. Wu, *Electrochim. Acta*, 56 (2011) 3071-3078.
26. Y. Huang, J. Chen, *Journal of Power Sources*, 195 (2010) 8267-8274.
27. Q. Q. Qiao, H. Z. Zhang, *J. Mater. Chem.*, A1 (2013) 5260-5265.
28. B. J. Sadeghi, *Chin. Chem. Soc.*, 60 (2013) 218-222.
29. S. H. Kang, M. M. Thackeray, *Electrochemistry Communications*, 11 (2009) 748-751.
30. G. Xu, J. Li, *Electrochim. Acta*, 117 (2014) 38-43.
31. Y. K. Sun, M. J. Lee, *Advanced Materials*, 24 (2012) 1192-1196.
32. X. Liang, H. Wu, *Int. J. Electrochem. Sci.*, 11 (2016) 5829-5837.
33. H. Meng, L. Li, *J. Alloys and Compounds*, 690 (2017) 256-266.
34. P. Li, Y. Xia, *Journal of Power Sources*, 327 (2016) 273-280.
35. G. Hu, M. Zhang, *J. Alloys and Compounds*, 690 (2017) 589-597.
36. N. Ishida, N. Tamura, *Journal of Power Sources*, 319 (2016) 255-261.
37. E. V. Lanina, V. D. Zhuravlev, *Electrochim. Acta*, 212 (2016) 810-821.
38. X. Yuan, Q. Xu, *Electrochim. Acta*, 207 (2016) 120-129.